JOURNAL OF MATERIALS SCIENCE 28 (1993) 3900–3910

Effect of notching speed on dynamic fatigue behaviour of polyethylene terephthalate polymers

J. T. YEH*, Y. T. LIN
Department of Textile Engineering, National Taiwan Institute of Technology Taipei, Taiwan 106

The influence of notching speed on the fatigue behaviour of crystalline and amorphous polyethylene terephthalate (PET) was investigated. A clear precrack adjacent to the notch tip was found after each crystalline sample was notched, and the precrack length increased when the samples were notched at higher speeds. The failure time, t_f, decreased significantly for samples with longer precrack lengths, and the decrease in t_f due to faster notching speeds was significantly lower for samples of high average molecule weight and calculated tie-molecule density. In contrast, a heart-shaped damaged structure surrounding the notch tip was observed after each amorphous sample was notched, and the size of the damaged zone, adjacent to the notch tip, increased significantly with the notching speed. Furthermore, the time to failure of each amorphous sample increased significantly as the notching speed increased. In fact, most of the increase in t_f is due to an increase in the initiation period, t_i. This significant increase in t_i is attributed to the larger damaged zone caused by higher notching speeds.

1. Introduction

The fatigue behaviour of polymeric materials has been studied for many years [1, 2]. Failure in this mode normally involves an initiation stage before perceivable crack growth can be observed. The initiation is important, because the initiation stage may be a significant portion of the total time-to-failure. For instance, much work has been done by Brown and coworkers on the slow crack growth of polyethylenes [3–10], and it was found that the time to initiate fracture is about 30–60% of the time-to-failure. In order to study crack initiation, a notch must be made on the specimen. Although razor blades are used by many researchers for making these notches, little information is available in the literature about the details of this art. In fact, the initiation data associated with these specimens are often discarded due to their poor reproducibility. One of the reasons for this poor reproducibility is that different notching procedures were used, and hence different microscopic events took place at the root of a notch prior to crack growth. Therefore, in order to produce consistent data on crack initiation in polymeric materials, a standard notching procedure must be made.

Extensive work has been done by Brown and coworkers [3–10] on the slow crack growth in polyethylene using a standard notching procedure: carefully controlling a razor blade at a rate of 50 $\mu m\,min^{-1}$ at room temperature, to produce the notch. It was found by Lu and Brown [6] that the scatter in failure time and crack-growth rates was reduced to $\pm$ 20%, which is excellent in comparison to the scatter reported in most other laboratories, as much as $\pm$ 100%. Recently, Lu, Qian and Brown [10] investigated the effect of various notching methods on the lifetime of slow crack failure at 80 °C for a tough-gas-pipe grade of polyethylene. However, specimens prepared with a rotary cutter provided a much longer failure time than those prepared by the standard procedure. This was explained [10] by the fact that a rotary cutter creates a rounder notch than the notch created by the standard procedure, and the large radius of curvature at the base of the notch results in a lower stress concentration. Another possible reason for this is that the "advancing" speed of a rotary cutter is faster than in the standard procedure, and hence rotary cutting results in a stronger damaged-zone structure, adjacent to the notch, than in samples prepared by the standard procedure. Therefore, a much longer failure time was found for samples prepared by the rotary cutter. However, little information is available in the literature about the microscopic events that occur prior to crack growth for samples notched at varying speeds.

In this work, the standard notching procedure suggested by Brown and coworkers [3–10] was used to notch three different molecular weight, $\bar{M}_w$, PET polymers. In addition to crystalline PET specimens, transparent amorphous specimens were prepared to observe the microscopic events occurring at the notch root prior to observable crack growth. The notching speed was found to dramatically influence the damaged-zone structure adjacent to the notch tip and

*To whom correspondence should be addressed.

0022–2461

to influence the subsequent dynamic fatigue properties of these specimens. In addition, samples with different $\bar{M}_w$ were also found to exhibit different responses to the notching speeds.

2. Experimental procedure

2.1. Materials

Shinite® PET resins were obtained (from Shinkong Synthetic Fibers Corporation, Taiwan). Before sample preparation, these resins were dried in a rotational vacuum oven at 150 °C for 8 h, cooled at room temperature and maintained in a vacuum desiccator.

2.2. Sample preparation

2.2.1. Crystalline PET samples

Dried resins A, B and C, described in Table I (see Section 3 for variable definitions), were prepared as rectangular plaques with dimensions of 10 × 90 × 90 mm at temperatures of 110 °C, 130 °C, and 130 °C, respectively, for 2 h. These injection-moulded plaques will be referred to as samples Ac, Bc and Cc, respectively. After the required crystallization time, the samples were air cooled. The plaques were then machined into compact-tension specimens (conducted under a plane-strain condition as suggested by ASTM standard E399-83 [11]) with dimensions of 40.0 × 38.4 × 8.0 mm.

2.2.2. Amorphous PET samples

A series of transparent amorphous specimens were made in order to observe the damaged zone formed during the notching procedure. These transparent specimens were prepared by injecting the dried resins A, B and C into a rectangular mould, and quenching them at 14.0 ± 0.5 °C for 15 min. The quenched amorphous plaques were then machined into compact-tension specimens [12] with dimensions of 40.0 × 38.4 × 4.0 mm. These quenched plaques will be referred to as samples Aa, Ba and Ca, respectively, in later discussion.

2.3. Notching procedure

Before the fatigue experiments, all the compact-tension specimens, prepared as in the previous section, were initially notched with a hacksaw to a length of 12.8 mm. The notch tip was then made by pressing a fresh razor blade into the inside surface of the specimens until an initial crack length of 13.2 mm was made. The razor blades were pressed at speeds ranging from 4–2000 μm min^{-1} at 25 °C. A fresh blade was used for each notch. The damaged-zone morphology adjacent to the prenotch was viewed through an Olympus SZ-40 optical microscope equipped with a PM-10AK photomicrographic system.

2.4. Characterization

2.4.1. Molecular weight and molecular weight distribution

The molecular weight and its distribution associated with PETs were determined by gel-permeation chromatography (GPC). Two 5 μm highly crosslinked ST-DVB copolymer columns ($10^3 + 10^4$ nm) were chosen and slowly conditioned from toluene to chloroform and then to chloroform/hexafluoroisopropanol (98 : 2 vol %) [13]. A liquid-chromatography-precolumn filter was placed in front of the first column to minimize contamination. The samples were prepared by dissolving in pure hexafluoroisopropanol (HFIP) and diluting with chloroform to reach a final concentration of 2 mg ml^{-1} in the chloroform/HFIP mixture (98 : 2 vol %) [13].The amount injected was 0.1 ml; the solvent flow was 1 ml min^{-1} at 30 °C. Specified molecular weights of narrow fractions of polystyrene were used to calibrate the instrument. Various molecular weight averages (i.e., $\bar{M}_n$, $\bar{M}_w$ and $\bar{M}_v$, where the subscripts denote number density, weight and volume averages) are summarized in Table II.

TABLE I Microstructural characterization

Resin	Sample	M_w	Thermal history	D (μm)	W_c (%)	L (nm)	f_T
A	Ac	75000	Isothermal crystallization at 130 °C, 2 h	15 ± 1	46.1	8.8	5.66
B	Bc	68000	Isothermal crystallization at 130 °C, 2 h	15 ± 3	46.5	8.9	5.29
C	Cc	46000	Isothermal crystallization at 110 °C, 2 h	15 ± 2	45.6	8.9	3.00
A	Aa	75000	Quench at 14 °C, 15 min	–	< 2.0	–	–
B	Ba	68000	Quench at 14 °C, 15 min	–	< 2.0	–	–
C	Ca	46000	Quench at 14 °C, 15 min	–	< 2.0	–	–

TABLE II Molecular weights associated with each resin

Resin	$\bar{M}_n$	$\bar{M}_w$	$\bar{M}_v$
A	41000	75000	70000
B	39000	68000	63000
C	28000	46000	43000

2.4.2. Thermal analysis

The melting behaviours and the degrees of crystallinity of all samples were studied by using a Dupont differential scanning calorimeter (DSC) model 2000. Baselines used in the experiments were adjusted to have a maximum fluctuation of less than 0.04 mW over the temperatures range of interest. With these baselines, the maximum variation of the heat of fusion was normally around $\pm 3 \times 10^3$ J kg^{-1}, which resulted in a $\pm 2\%$ error in estimating the percentage crystallinity, W_c. The instrument was calibrated using pure indium. All the scans were carried out under flowing nitrogen (25 ml min^{-1}).

The degrees of crystallinity of all the samples were estimated using baselines drawn from 90 to 280 °C and a perfect-crystal heat of fusion of 144×10^3 J kg^{-1} [14]. Typical sample masses used in the DSC experiments were 10 mg for the determination of the degree of crystallinity and 0.5×10^{-6} kg for the melting point, T_m, measurement. For samples of this size and mass, a maximum variation in T_m of ± 0.5 °C was normally observed. All scans were carried out at a heating rate of 40 °C min^{-1}. At least three samples from each specimen type were tested.

Lamellar thickness was not measured directly, but was estimated from the observed melting temperature using the Gibbs–Thomson equation [15]. Values of 1.455×10^3 kg m^{-3} for the perfect-crystal density [16], 50×10^{-3} J m^{-2} for the end-surface free energy [17], and 280 °C for the equilibrium melting temperature [17] were used in the calculation of lamellar thickness.

2.4.3. Supermolecular structure and size

The supermolecular structure of all samples was viewed through a crossed polarizer with an Olympus BHSP-300 optical microscope, equipped with a PM-10 AK photomicrographic system. Sections 10 mm thick were cut at room temperature from test pieces of PET plaques using a Reichert-Jung Ultracut E Microtome equipped with a glass knife. By drawing lines across the micrograph of each sample, the average sizes of the supermolecular structures can then be calculated as the ratio of the total lengths of the lines to the total number of supermolecular structures. Normally, three lines were drawn for each estimation. The spherulite-size distribution of these samples are represented by the average spherulite diameter, D, together with its standard deviation.

2.4.4. Tie-molecule density

In the past, tie molecules have been characterized by using such techniques as transmission electron microscopy [18–25], neutron scattering [26], nuclear magnetic resonance [27], and by measurement of the brittle-fracture strength [28]. However, due to the small dimensions and complexity of the intercrystalline links, these techniques (excluding the last one) do not appear to be suitable for ready analysis of a relatively large number of bulk samples. In fact, the sensitivity of the method based on brittle-fracture-stress measurements is also limited in distinguishing samples with relatively small differences in tie-molecule density [29]. In this study, we used the chain dimensions of the polymers to estimate the number of tie molecules formed per chain as suggested recently by Yeh and Runt [29]. Although this model is an indirect and qualitative approach for estimating the number of tie molecules, it still allows comparison and ranking of a series of samples. As will be seen, these predictions are consistent with the observed changes in mechanical behaviour.

The model allows evaluation of "conventional" tie molecules as well as "entangled" tie molecules. The number of "conventional" tie molecules formed per chain, $T_1(M)$, in a monodispersive polymer is given as:

$$T_1(M) = \tfrac{1}{3}[\int_{2.45Lp}^{\infty} a' I(r,Lp)\, r^2 \exp(-(b')^2 r^2)\mathrm{d}r] \quad (1)$$

The number of "entangled" tie molecules formed per chain, $T_2(M)$, in a monodispersive polymer is given as

$$T_2(M) = [\int_{1.22Lp}^{\infty} N a' r^2 \exp(-(b')^2 r^2)\mathrm{d}r] \quad (2)$$

$$N = I(V_M/V_{M_c}) \quad (3)$$

Where, Lp is the long period. a' and b' are constants. $I(r,Lp)$ is an integer function which takes into account the increasing probability of forming tie molecules with increasing radius of gyration. r is the end-to-end distance of random coil in the melt. N is the number of entanglements per chain after crystallization, and is assumed to be proportional to the hydrodynamic volume of the molecular chains. $I(V_M/V_{M_c})$ is the integer part of (V_M/V_{M_c}). V_M and V_{M_c} are the hydrodynamic volumes of the polymer chain with given molecular weights of M and M_c, respectively. M is the molecular weight per chain in a monodispersive polymer. M_c is the critical molecular weight at which the dependence of viscosity on molecular weight changes from an exponent of 1–3.4. For PET, M_c is selected to be 13700, which corresponds, approximately, to 700 main-chain atoms [30].

The overall number of tie molecules formed per chain, $T(M)$, of molecular weight M is then equal to

$$T(M) = T_1(M) + T_2(M) \quad (4)$$

Bulk polymers are not generally monodispersive, and the actual probability of forming a tie-molecule per chain must be calculated from the overall molecular-weight distribution of a given polymer, i.e. the average number of tie molecules formed per chain must be calculated from the summation of the product of $T(M)$ and the percentage of each monodispersive polymer in the distribution.

2.5. Fatigue crack propagation

All fatigue experiments were performed on a Material

Test System (MTS model 810), using a sinusoidal waveform, a minimum-to-maximum-load ratio, R, of 0.1 and a frequency of 1 Hz. The maximum loads were 70 kg, 40 kg, 25 kg, 35 kg, 30 kg and 20 kg for samples Ac, Bc, Cc, Aa, Ba and Ca, respectively. An Olympus SZ-40 optical microscope connected to a Hitachi CCTV camera (model HV-7200), and an Emersion video-cassette recorder, were used to monitor and record the crack length. Plots of the crack length, a, versus fatigue cycle, N, are used to compare the fatigue behaviour of different samples.

2.6. Fracture-surface morphology

Fatigue fracture surfaces were examined using a JOEL JSM-5200 scanning electron microscope. Prior to scanning-electron-microscopy (SEM) examination, all specimens were coated by a vacuum-evaporated layer of gold for about 12 s at 10 mA. As will be discussed later, all the fracture surfaces revealed a clear demarcation region between the region of slow crack growth and the notch root. Additionally, a parabolic crack front was also observed in the demarcation region of each sample. Following the procedure in an ASTM specification [11] the length of this demarcation region was evaluated as the arithmetic average of the lengths measured in the following three positions: the centre of the crack front, midway between the centre of the crack front and its end at the surface, and the end of each surface of the specimen. At least three samples of each specimen were evaluated.

3. Results and discussion

3.1. Crystalline microstructure

Microstructural characterization of all of the samples is summarized in Table I. These samples can be grouped into two types according to the percentage crystallinity. The first three samples Ac, Bc, and Cc are of crystalline type. Approximately the same percentage crystallinity, W_c, lamellar thickness, L, and average spherulite diameter, D, were found for samples Ac, Bc and Cc. A typical value for L is approximately 9 nm. Fig. 1 shows typical optical micrographs of these specimens; the average spherulite diameter was around 15 μm. Tie-molecule densities, f_T, predicted from the chain dimensions of the series are summarized in Table I. The predicted values are 5.66, 5.29 and 3.00 for samples Ac, Bc and Cc, respectively. This evaluation predicts an increase in the number of tie molecules formed per molecular chain with increasing molecular weight, which qualitatively agrees with expectation [19, 29, 31–34]. The other three samples Aa, Ba and Ca are of amorphous type. Their molecular weights are the same as their crystalline counterparts, but with approximately 0% crystallinity, due to their thermal history.

3.2. Characterization of damaged-zone morphology adjacent to the notch tip

3.2.1. Crystalline PET samples

A clear precrack adjacent to the notch tip was found after each crystalline sample was notched at the notching speeds used in this study. Fig. 2 shows typical optical micrographs revealing the damaged-zone structure adjacent to the notch tip of samples Ac, Bc and Cc. The crystalline samples were too brittle to prevent the formation of a precrack even when samples were notched at a relatively slow speed (e.g. 4 μm min^{-1}). The fracture surfaces of each crystalline sample after fatigue fracture are shown in Figs 3–5. It is interesting to note that a clear demarcation region was found between the region of slow crack growth and the notch root of each specimen. The precrack lengths on the edges of the fracture surfaces are similar to those observed in the optical micrographs (Fig. 2). Thus, it is reasonable to believe that the clear demarcation regions are the corresponding remnants of the precrack regions. As shown in Fig. 6, the precrack length evaluated from the fracture surface increased when the crystalline samples were notched at higher speeds. This is probably because a larger stress is encountered locally at the notch tip as the notching speed is increased, and, hence, a longer precrack length results.

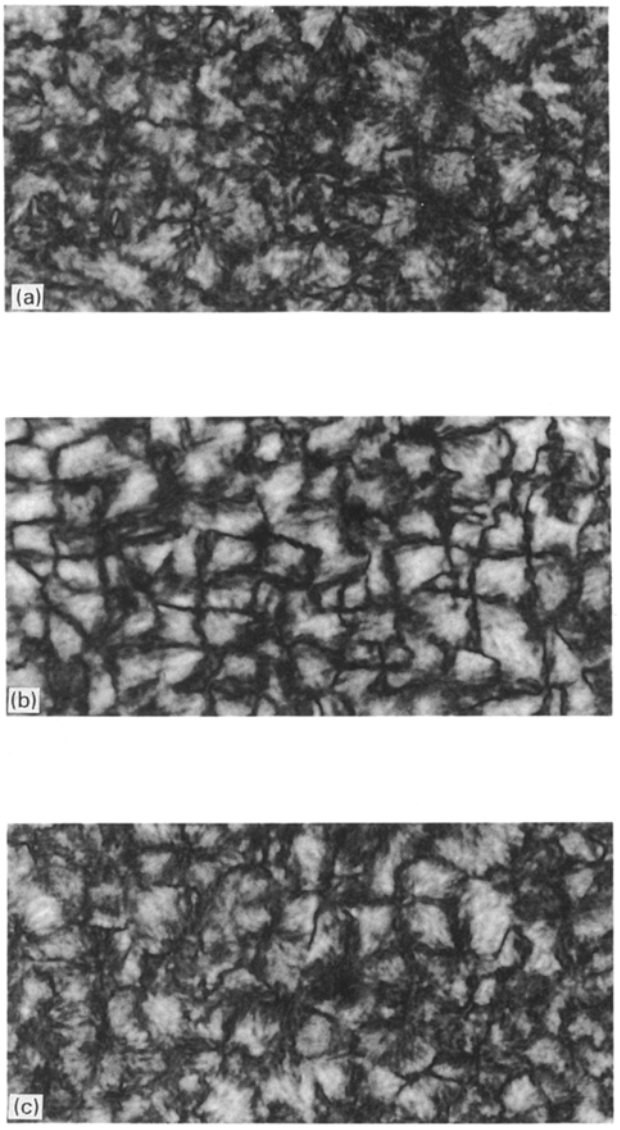

Figure 1 Optical micrographs: (a) sample Ac, (b) Bc, and (c) Cc.

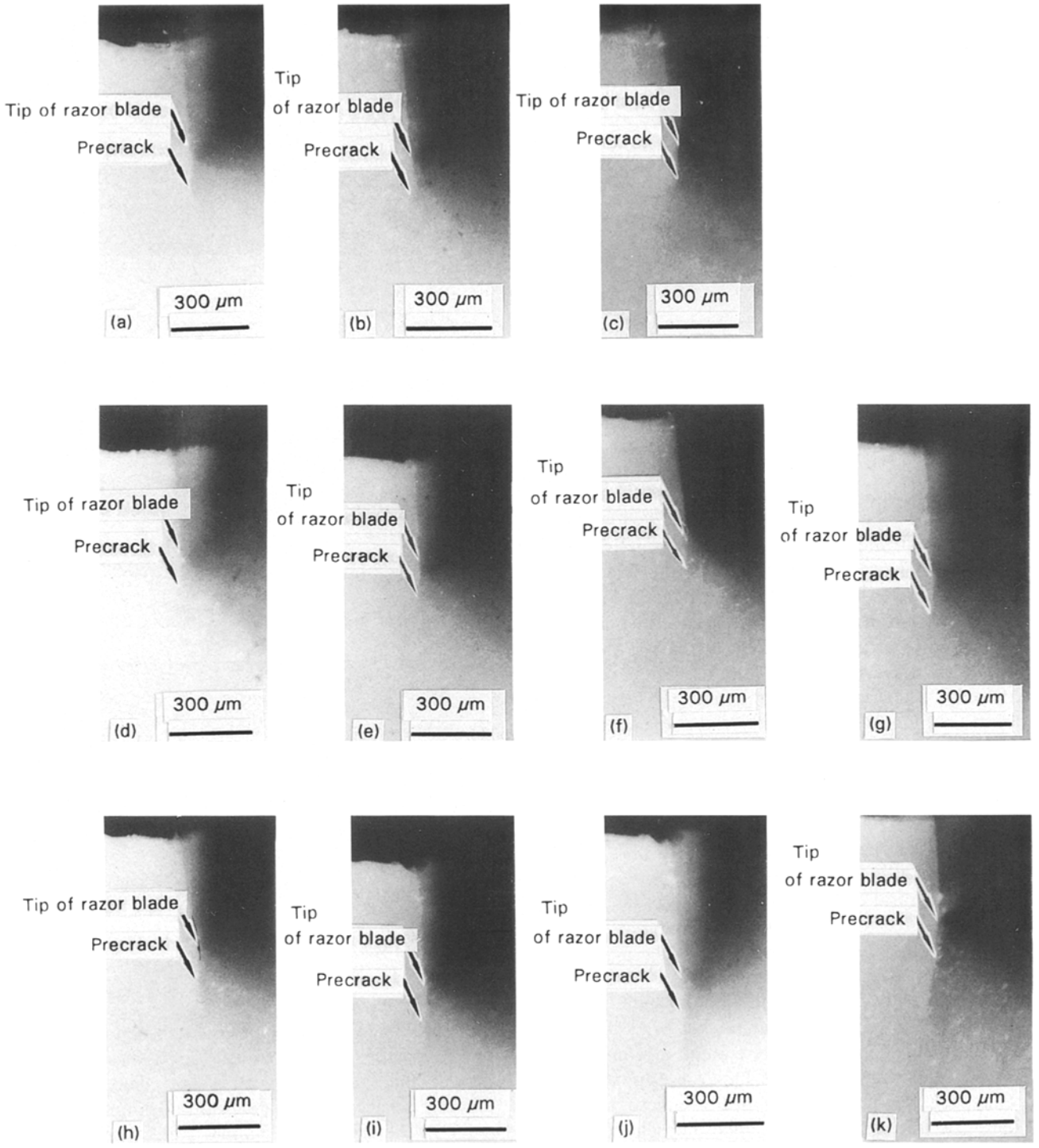

Figure 2 Optical micrographs revealing the damaged-zone structure adjacent to the notch tip of samples Ac, Bc and Cc notched at different speeds to a depth of 0.4 mm: (a) Ac, 4 μm min^{-1}; (b) Ac, 40 μm min^{-1}; (c) Ac, 2000 μm min^{-1}; (d) Bc, 4 μm min^{-1}; (e) Bc, 40 μm min^{-1}; (f) Bc, 400 μm min^{-1}; (g) Bc, 2000 μm min^{-1}; (h) Cc, 4 μm min^{-1}; (i) Cc, 40 μm min^{-1}; (j) Cc, 400 μm min^{-1}; and (k) Cc, 2000 μm min^{-1}.

3.2.2. Amorphous PET samples

Instead of forming a precrack adjacent to the notch tip, a heart-shaped damaged structure surrounding the notch tip was found after each amorphous PET sample was notched. Typical optical micrographs showing the heart-shaped damaged structure of the amorphous sample are shown in Fig. 7. The SEM micrographs corresponding to the fracture surface of each sample notched at varying speeds are shown in Figs 8–10. The resulting fracture surface of each amorphous specimen revealed a clear demarcation region between the region of slow crack growth and the notch root, similar to that of the crystalline specimens. In addition, the size of this demarcation region is similar to that observed adjacent to the notch tip from the optical micrographs. Therefore, it is reasonable to believe that the clear demarcation region is the remnant of the damaged zone adjacent to the notch tip after notching. In fact, the size evaluated from the fracture surface of the damaged zone adjacent to the notch tip increased significantly with increasing notching speed (see Fig. 11). Detailed transformation mechanisms accounting for the formation of this damaged-zone structure are not clear. However, the

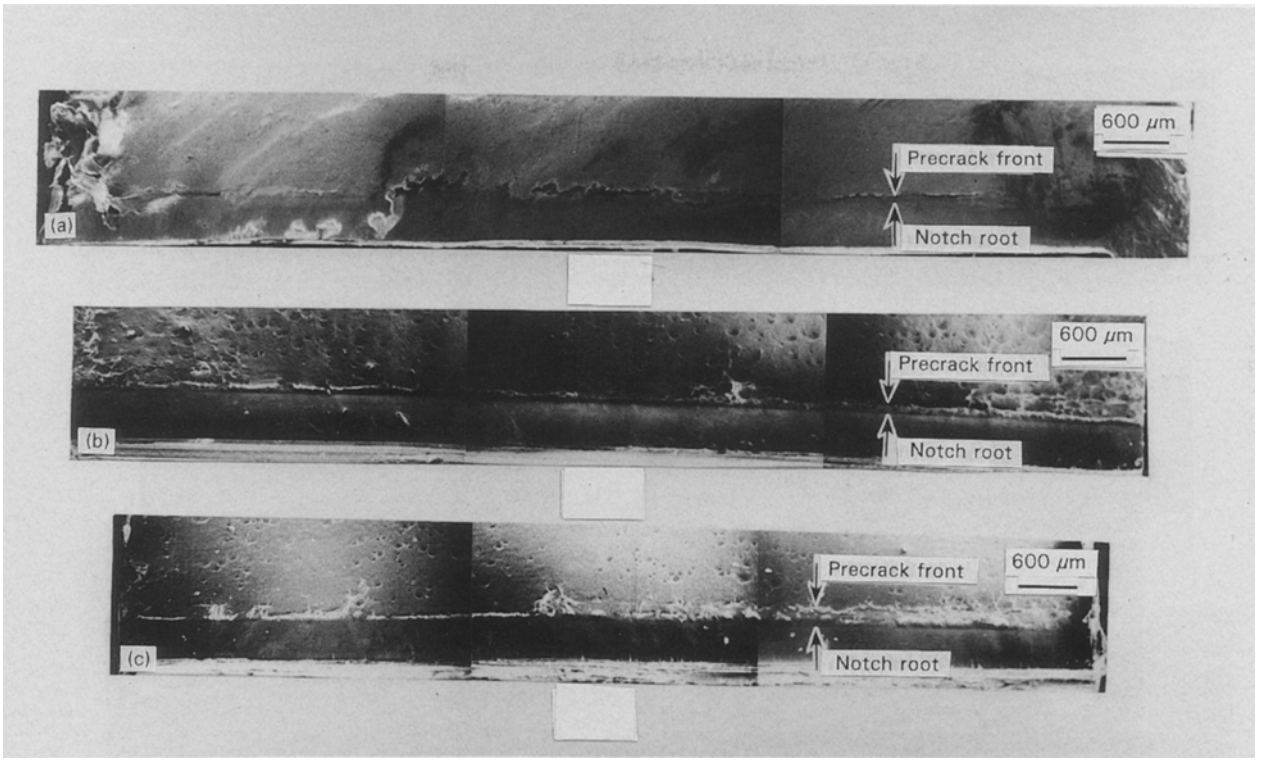

Figure 3 Fracture surfaces of sample Ac notched at a speed of: (a) 4 μm min^{-1}, (b) 40 μm min^{-1}, and (c) 2000 μm min^{-1}.

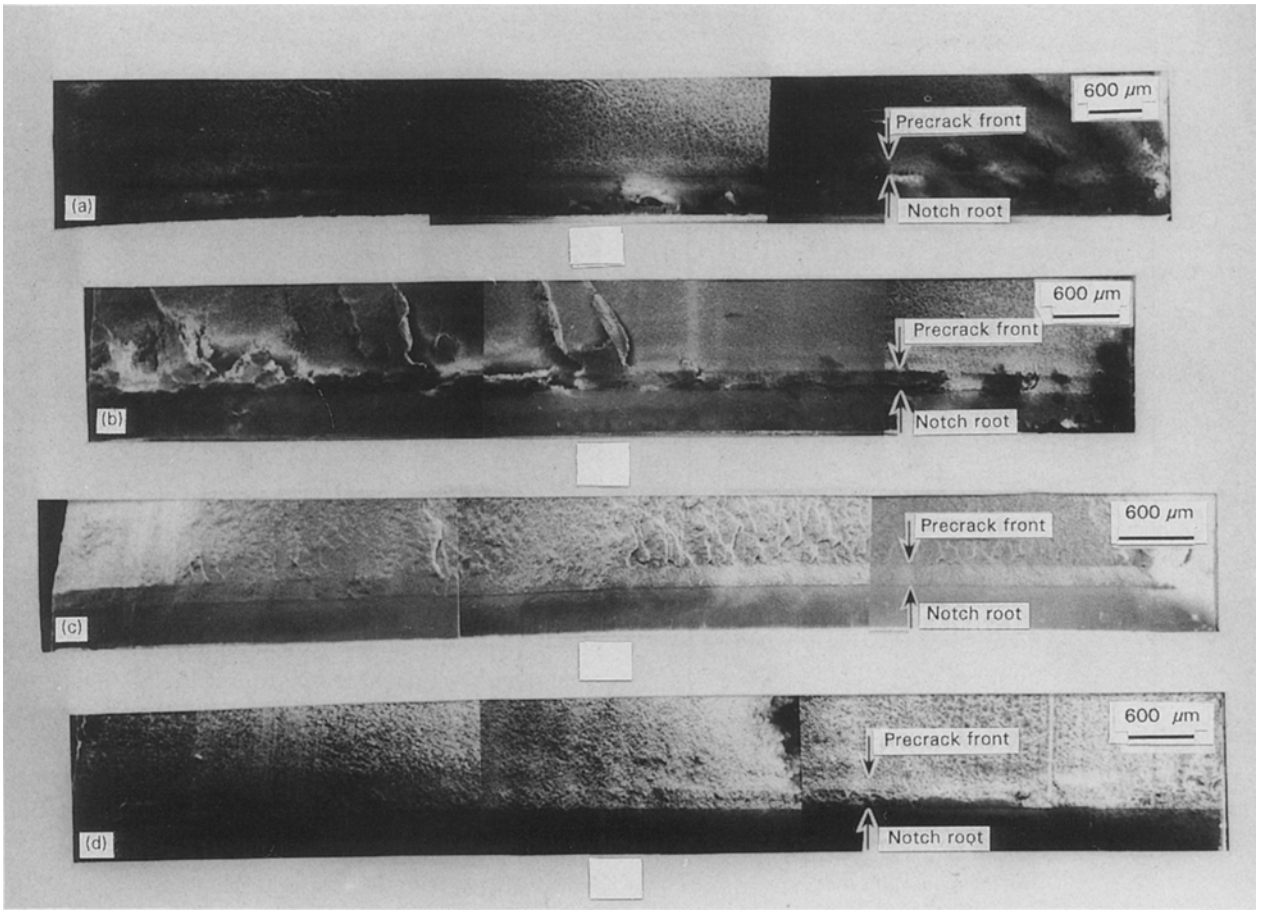

Figure 4 Fracture surfaces of sample Bc notched at a speed of (a) 4 μm min^{-1}, (b) 40 μm min^{-1}, (c) 400 μm min^{-1}, and (d) 2000 μm min^{-1}.

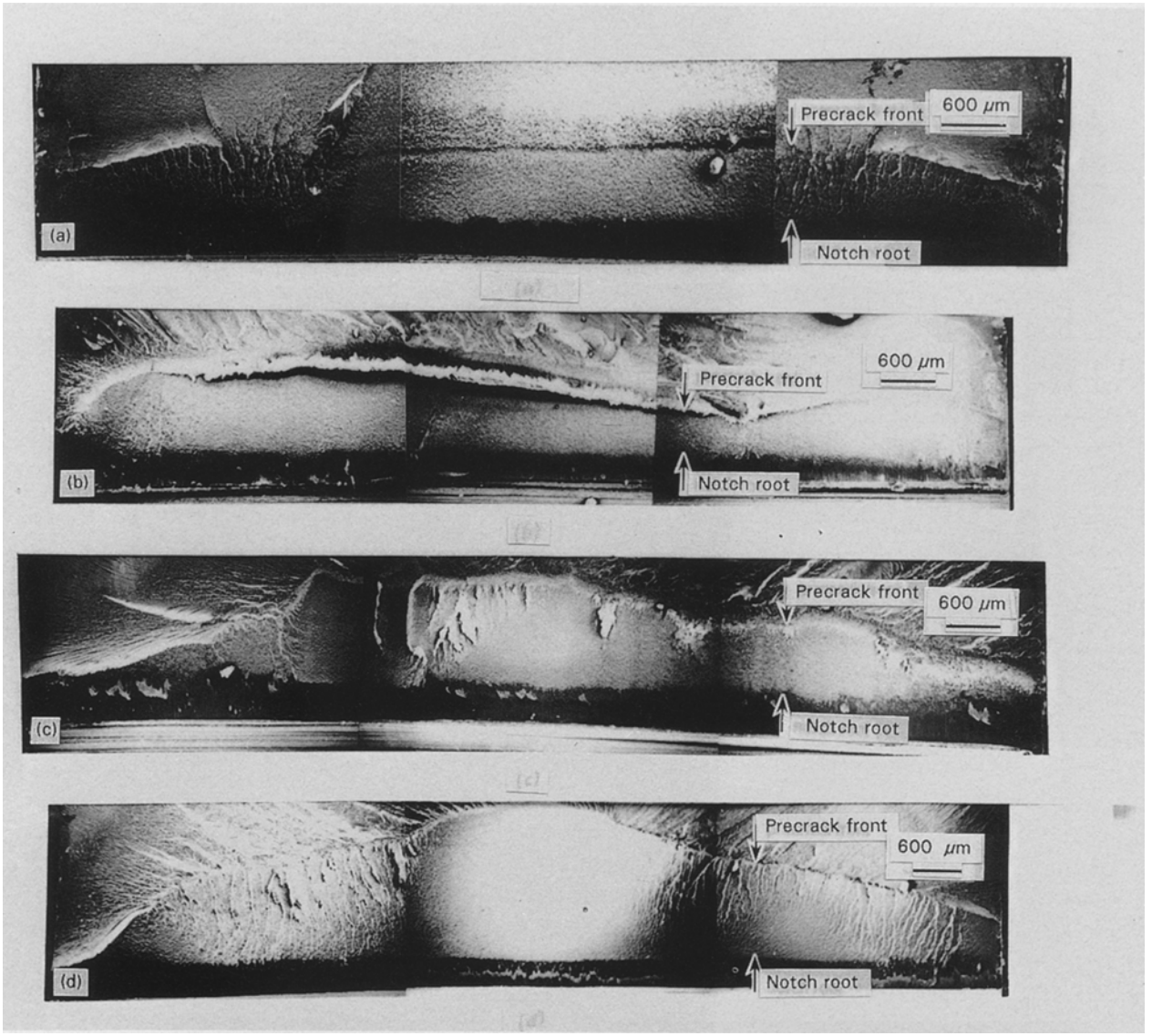

Figure 5 Fracture surfaces of sample Cc notched at a speed of: (a) 4 μm min^{-1}, (b) 40 μm min^{-1}, (c) 400 μm min^{-1}, and (d) 2000 μm min^{-1}.

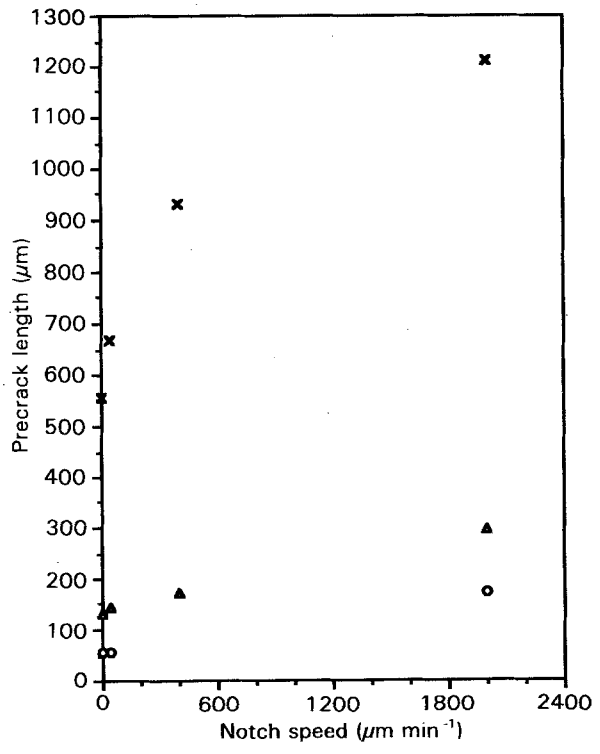

Figure 6 Precrack lengths notched at varying speeds for samples: (○) Ac, (△) Bc, and (×) Cc.

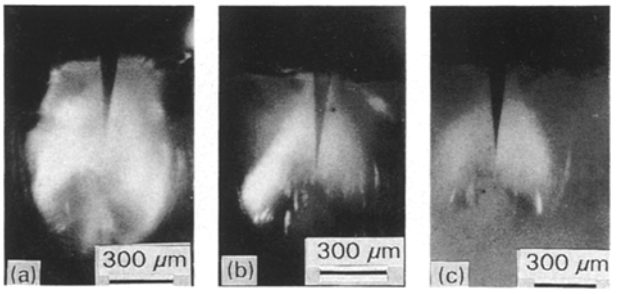

Figure 7 Optical micrographs revealing the damaged-zone structure adjacent to the notch tip of samples notched at a speed of 2000 μm min^{-1}: (a) Aa, (b) Ba, and (c) Ca.

percentage crystallinity associated with the damaged-zone structure increased by around 10.0%. Therefore, it is reasonable to suggest that stress-induced crystallization may occur during the notching process, and, hence, a larger damaged zone results as the stress at the notch tip increases with increasing notching speed.

3.3. Fatigue crack propagation

3.3.1. Crystalline PET samples

Plots of crack length, a, against fatigue cycle, N, of the

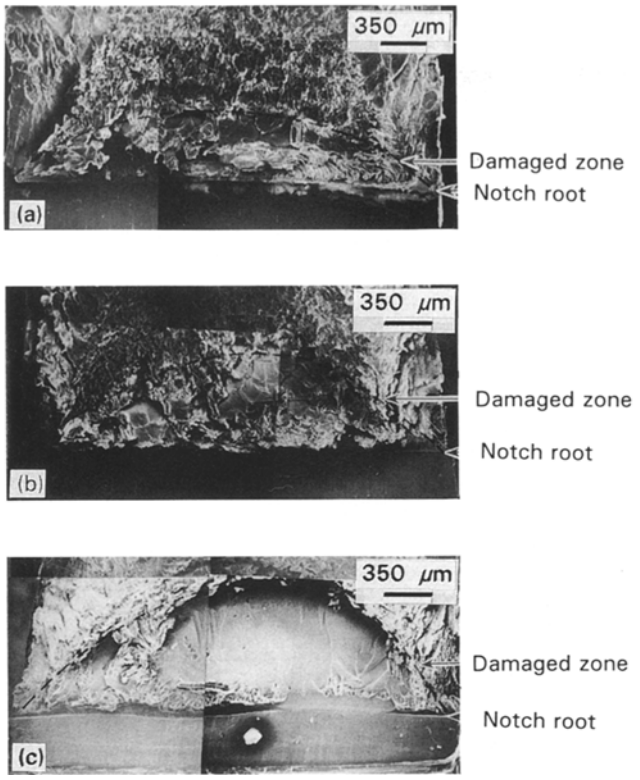

Figure 8 Fracture surfaces of sample Aa notched at a speed of: (a) 4 μm min^{-1}, (b) 400 μm min^{-1}, and (c) 2000 μm min^{-1}.

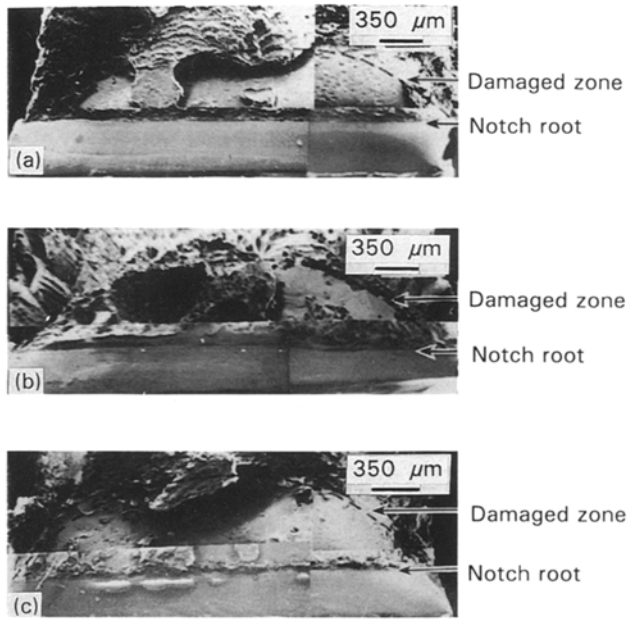

Figure 9 Fracture surfaces of sample Ba notched at a speed of (a) 4 μm min^{-1}, (b) 400 μm min^{-1}, and (c) 2000 μm min^{-1}.

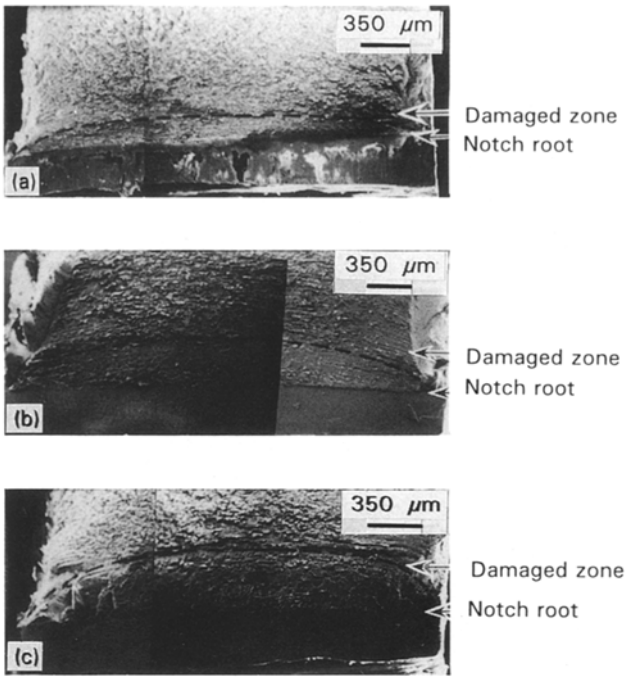

Figure 10 Fracture surfaces of sample Ca notched at a speed of (a) 4 μm min^{-1}, (b) 400 μm min^{-1}, and (c) 2000 μm min^{-1}.

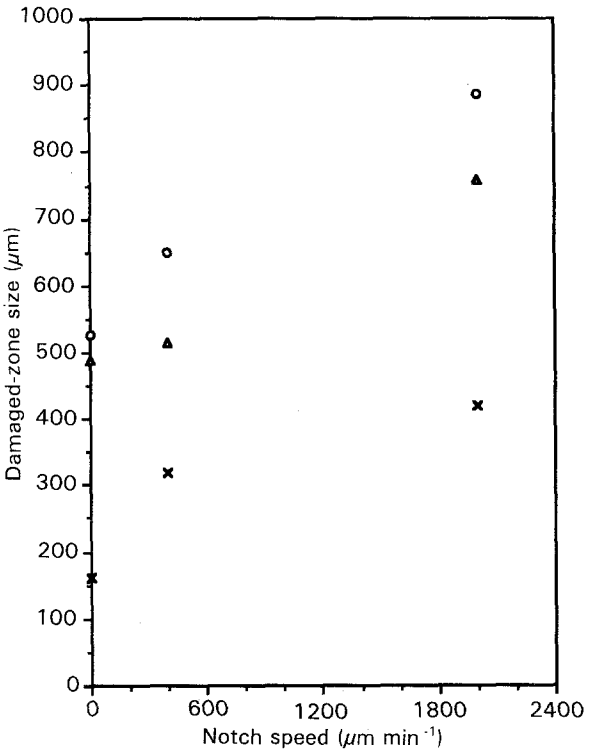

Figure 11 Damaged-zone size of samples notched at varying speeds: (○) Aa, (△) Ba, and (×) Ca.

crystalline samples are shown in Figs 12–14. At least three fatigue-crack-propagation experiments were performed on each sample type. Within experimental error, there is no significant difference in the time to failure, t_f, for sample Ac notched at 4 μm min^{-1} and 40 μm min^{-1} (see Fig. 12). However, t_f for sample Ac notched at 2000 μm min^{-1} reduced to approximately half (in around 6500 cycles) that of the samples notched at 4 μm min^{-1}. It is generally expected that t_f is shorter for samples associated with a longer initial crack length. Since the precrack length associated with sample Ac notched at 2000 μm min^{-1} is significantly longer than that of samples notched at 4 μm min^{-1} and 40 μm min^{-1} (see Fig. 6), this decrease in t_f is not unreasonable. As shown in Figs 13, 14, this decrease in t_f at faster notching speeds was also observed for samples Bc and Cc. However, a more significant decrease in t_f and increase in precrack length (see Fig. 6)

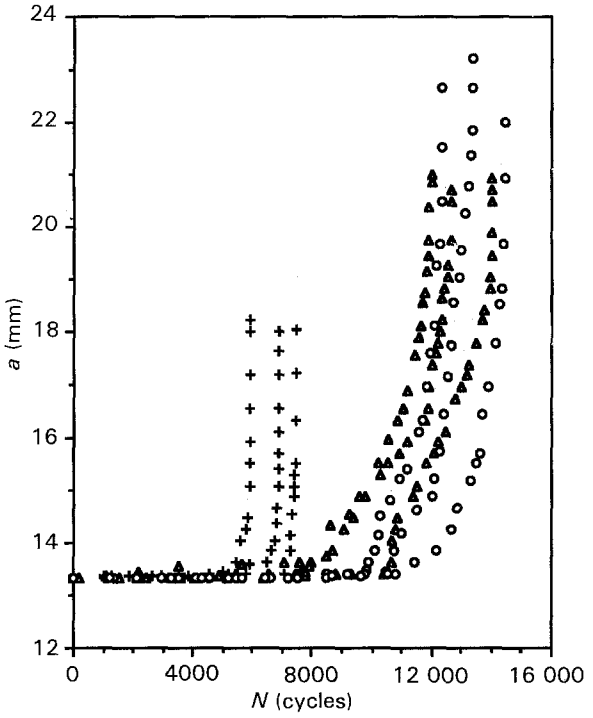

Figure 12 Crack length, a, plotted against fatigue cycle, N, for sample Ac notched at speeds of: (○) 4 μm min^{-1}, (△) 40 μm min^{-1}, and (+) 2000 μm min^{-1}.

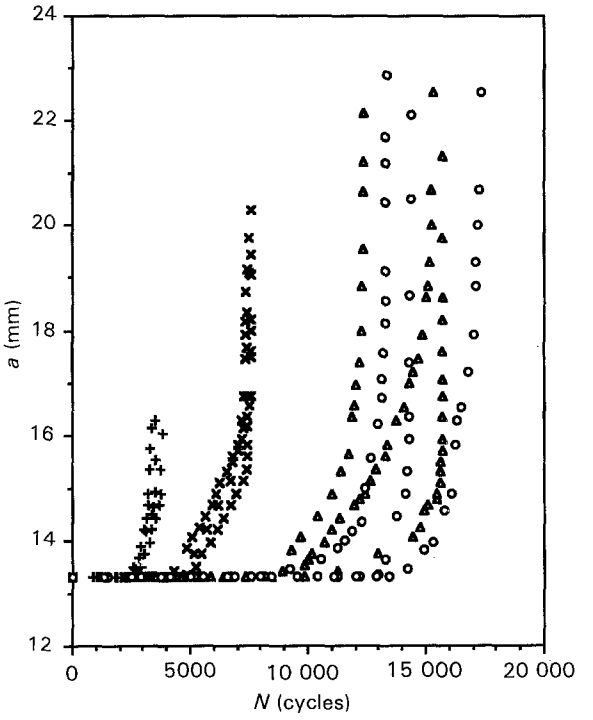

Figure 13 Crack length, a, plotted against fatigue cycle, N, for sample Bc notched at speeds of: (○) 4 μm min^{-1}, (△) 40 μm min^{-1}, and (+) 2000 μm min^{-1}.

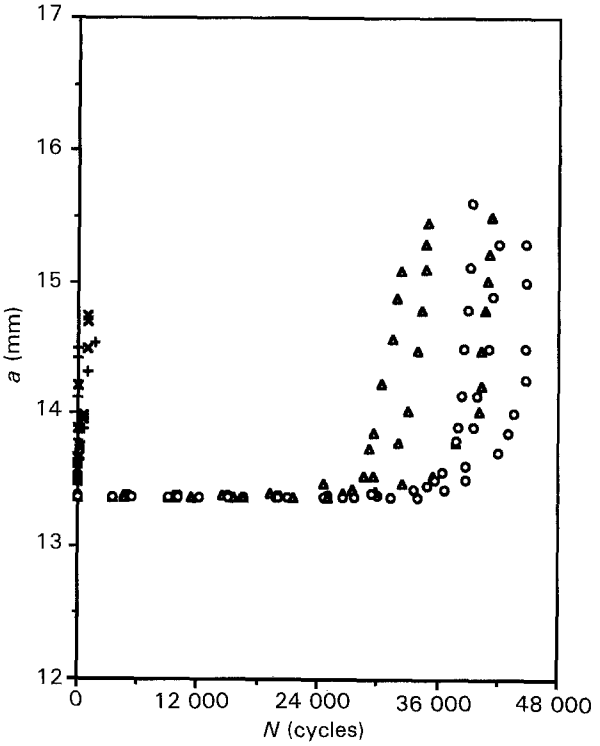

Figure 14 Crack length, a, plotted against fatigue cycle, N, for sample Cc notched at speeds of: (○) 4 μm min^{-1}, (△) 40 μm min^{-1}, (×) 400 μm min^{-1}, and (+) 2000 μm min^{-1}.

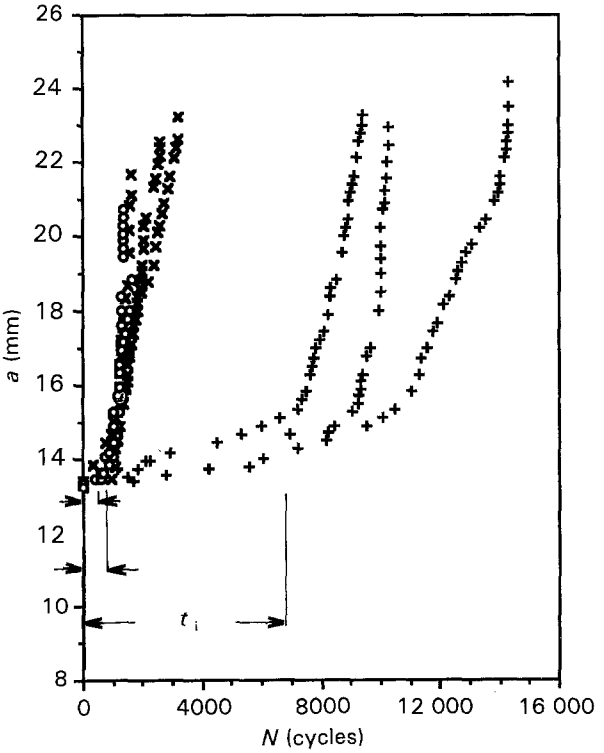

Figure 15 Crack length, a, plotted against fatigue cycle, N, for sample Aa notched at speeds of: (○) 4 μm min^{-1}, (×) 400 μm min^{-1}, and (+) 2000 μm min^{-1}. t_i is initiation period.

were observed for samples associated with lower weight-average molecular weights, $\bar{M}_w$. For instance, the t_f of samples Bc and Cc notched at 2000 μm min^{-1} reduced to around 1/4 and 1/450, respectively, of that of their corresponding samples notched at 4 μm min^{-1}. As mentioned previously, W_c, D and L within the series Ac, Bc and Cc remained unchanged and the estimated f_T increased with increasing weight-average molecular weight. It quickly becomes clear that the difference in the decrease of t_f due to faster notching reflects changes in $\bar{M}_w$ and f_T. These results can be reasonably explained by the idea that higher tie-molecule densities will lead to a more effective entanglement network in the notch-tip region and hence result in a shorter precrack length. Therefore, the reduction in t_f due to faster notching speeds

(higher stress) decreases significantly for samples with higher f_T.

3.3.2. Amorphous PET samples

Plots of a versus N of the amorphous series Aa, Ba and Ca are shown in Figs 15–17, respectively. In contrast to crystalline samples, the time-to-failure of the amorphous samples increased significantly as the notching speed increased. It is interesting to note that all the plots show an initiation period (as marked on the plots), in which the crack growth rate is very slow. In fact, the length of the initiation period, t_i, increases consistently with the notching speed, and the crack length in this period is approximately equal to the size of the damaged-zone evaluated from SEM micrographs (see Fig. 11). After the initiation period, the crack grew faster and the amounts of time before failure (i.e. $t_f - t_i$) for each of the samples notched at varying speeds are approximately the same. These results suggest that most of the increase in t_f with increasing notching speeds is due to the increase in t_i. As mentioned earlier, detailed transformation mechanisms accounting for the formation of the damaged-zone structure adjacent to the notch tip are not completely understood at this point. However, the results described above can be reasonably explained by the idea that the damaged-zone structure is more resistant to crack propagation than that of the original material, and hence a longer t_i results as the length of damaged-zone adjacent to the notch tip increases. However, since the propagating front will be preceded by the same deformation-zone structure after the crack propagates completely through the damaged zone, a result of approximately the same value, $t_f - t_i$, for each sample, notched at varying speeds, is not unreasonable.

4. Conclusions

The failure time, t_f, associated with the crystalline PET samples decreases significantly when the samples were notched at higher speeds. A clear precrack adjacent to the notch tip was found after each crystalline sample was notched, and the precrack length evaluated from the fracture surface increased when samples were notched at higher speeds. This significant change in t_f with notching speed reflects the change in precrack length of crystalline samples after the notching procedure. However, the reduction in t_f due to faster notching speeds decreased dramatically for samples with higher average molecular weight and calculated tie-molecule density. Instead of forming a precrack adjacent to the notch tip, a heart-shaped damaged structure surrounding the notch tip was observed after each amorphous sample was notched, and the size of the damaged-zone adjacent to the notch tip increased significantly with increasing notching speed. However, the failure time of each amorphous sample increased significantly as the notching speed increased. In fact, most of the increase in t_f is due to the increase in the initiation period, t_i. This significant increase in t_i is attributed to the larger damaged-zone size adjacent to the notch tip, which is more resistant to crack propagation than that of the original material.

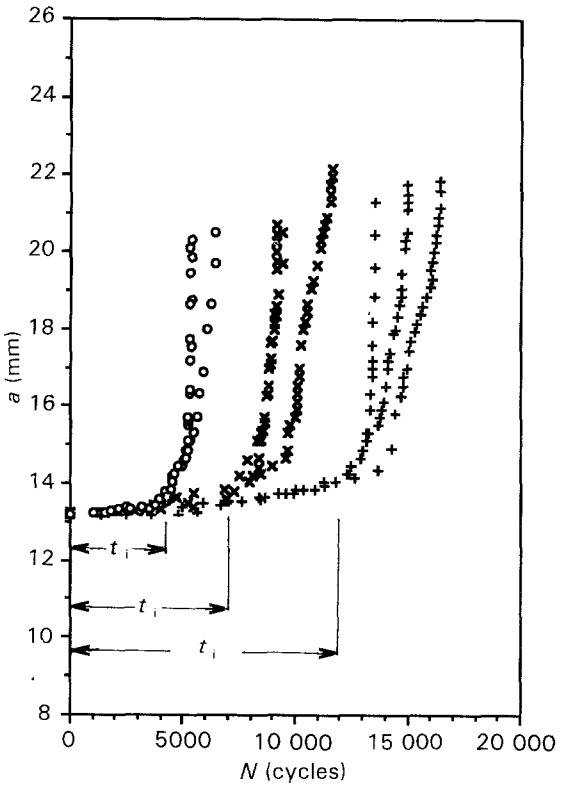

Figure 16 Crack length, a, plotted against fatigue cycle, N, for sample Ba notched at speeds of: (○) 4 μm min^{-1}, (×) 400 μm min^{-1}, and (+) 2000 μm min^{-1}. t_i is initiation period.

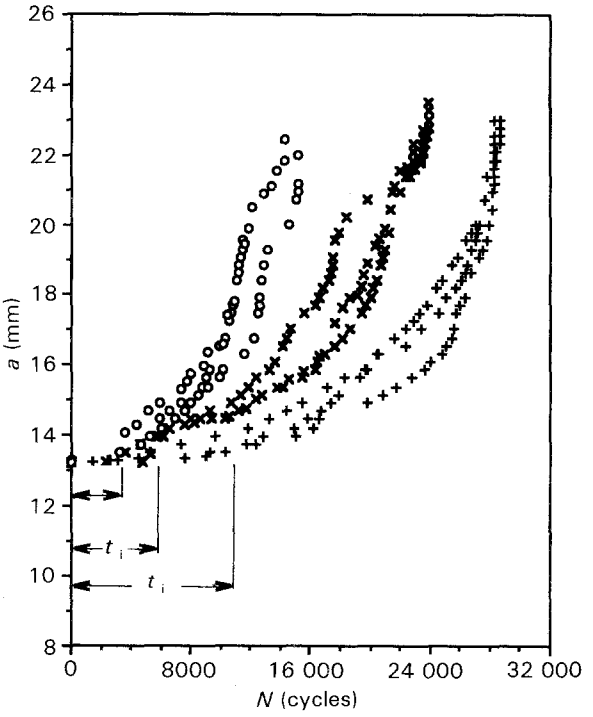

Figure 17 Crack length, a, plotted against fatigue cycle, N, for sample Ca notched at speeds of: (○) 4 μm min^{-1}, (×) 400 μm min^{-1}, and (+) 2000 μm min^{-1}. t_i is initiation period.

Acknowledgements

The authors express their appreciation to the National Science Council (Grant NSC 80-0405-E011-07) for

support of this work. Thanks are extended to Misses Ling-ya Wu and Mei-jen Yang for their assistance in preparation of this manuscript. Thanks are also extended to Shingkong Synthetic Fibers Corporation for supplying the PET resins. Last but not least, the authors also express their appreciation to Mr Bruce M. C. Lu of Yung Chia Chemical Industries Corporation for many helpful discussions of this work.

References

1. R. W. HERTZBERG and J. A. MANSON, in "Fatigue of engineering plastics" (Academic Press, New York 1980).
2. J. A. MANSON and R. W. HERTZBERG, *Ency. Polym. Sci. Engng.* **7** (1986) 378.
3. S. K. BHATTACHARYA and N. BROWN, *J. Mater. Sci.* **19** (1984) 2519.
4. S. K. BHATTACHARYA and N. BROWN, *J. Mater. Sci.* **20** (1985) 2767.
5. X. LU and N. BROWN, *J. Mater. Sci.* **21** (1986) 2423.
6. X. LU and N. BROWN, *J. Mater. Sci.* **21** (1986) 4081.
7. X. LU, X. WANG and N. BROWN, *J. Mater. Sci.* **23** (1988) 643.
8. N. BROWN and X. WANG, *Polymer* **29** (1988) 463.
9. Y. HUANG and N. BROWN, *J. Mater. Sci.* **23** (1988) 3648.
10. X. LU, R. QIAN and N. BROWN, *J. Mater. Sci* **26** (1991) 881.
11. Plane-Strain Fracture Toughness of Metallic Materials, *ASTM E399–83*, (American Society for Testing and Materials, Philadelphia 1989).
12. Measurement of Fatigue Crack Growth Rates, *ASTM E647–88a*, (American Society for Testing and Materials, Philadelphia, 1989).
13. K. WEISSKOPF, *J. Polym. Sci., A* **26** (1988) 1919.
14. P. E. SLADE, T. A. ORFINO, in "Analytical calorimetry", edited by R. S. Porter, J. F. Johnson, (Plenum Press, New York, 1968) p. 63.
15. J. D. HOFFMAN, G. T. DAVIS and J. I. LAURITZEN, "Treatise on solid state chemistry", Vol. 3, edited by N. B. Hannyay (Plenum Press, New York, 1975).
16. R. de P. DAUBENY, C. W. BUNN, C. J. BROWN, *Proc. Roy. Soc. A* **226** (1954) 531.
17. G. C. ALFONSO, E. PEDEMONTE and L. PONZETTI, *Polymer* **20** (1979) 104.
18. H. D. KEITH, F. J. PADDEN Jr, and R. G. VADIMSKY, *J. Polym. Sci., A-2* **4** (1966) 267.
19. H. D. KEITH, F. J. PADDEN Jr, and R. G. VADIMSKY, *J. Appl. Phys.* **37** (1966) 4027.
20. H. D. KEITH, F. J. PADDEN Jr, and R. G. VADIMSKY, *J. Appl. Phys.* **42** (1971) 4585.
21. R. G. VADIMSKY, H. D. KEITH, and F. J. PADDEN, *J. Polym. Sci., A-2* **7** (1969) 1367.
22. H. A. DAVIS, *J. Polym. Sci. A-2* **4** (1966) 1009.
23. S. NAGOU and K. AZUMA, *J. Macromol. Sci., Phys. Ed.* **16** (1979) 435.
24. E. S. CLARK, *S. P. E. J.* **23** (1967) 46.
25. H. D. KEITH, F. J. PADDEN, Jr., and R. G. VADIMSKY, *J. Polym. Sci., Polym. Phys. Ed.* **18** (1980) 2307.
26. E. W. FISCHER, K. HAHN, J. KUGLER, U. STRUTH, and R. BOM, *J. Polym. Sci., Polym. Phys. Ed.* **22** (1984) 1491.
27. V. V. ZHIZHENKOV and E. A. EGOROV, *J. Polym. Sci., Polym. Phys. Ed.* **22** (1984) 117.
28. N. BROWN and I. M. WARD, *J. Mater. Sci.* **18** (1983) 1413.
29. J. T. YEH and J. RUNT, *J. Polym. Sci., Polym. Phys. Ed.*, **29** (1991) 371.
30. W. W. GRAESSLEY, *Adv. Polym. Sci.* **16** (1974) 55.
31. J. T. YEH and J. RUNT, *J. Mater. Sci.* **24** (1989) 1421.
32. Y. L. HUANG and N. BROWN, *J. Mater. Sci.* **23** (1991) 3648.
33. Y. L. KEITH, F. J. PADDEN, Jr., and R. G. VADIMSKY, *J. Appl. Phys.* **42** (1971) 4585.
34. S. WELLINGHOFF and E. BAER, *J. Macromol. Sci. Phys. B* **11** (1975) 367.

Received 23 June
and accepted 21 October 1992